engineering proceedings

MDPI

Proceeding Paper

Hydrothermal Synthesis of Mesoporous $FeTiO_3$ for Photo-Fenton Degradation of Organic Pollutants and Fluoride Adsorption †

Neha Gupta [1], Arpita Sarkar [2], Bivek Pradhan [1] and Soumya Kanti Biswas [1,*]

[1] Department of Chemistry, Sikkim Manipal Institute of Technology, Sikkim Manipal University, Majhitar 737136, Sikkim, India; neha_20211009@smit.smu.edu.in (N.G.); pradhanbivek44@gmail.com (B.P.)
[2] Department of Chemistry, School of Basic Sciences, Swami Vivekananda University, Barrackpore, Kolkata 700121, West Bengal, India; 80.arpita@gmail.com
* Correspondence: soumya.biswas@smit.smu.edu.in
† Presented at the International Conference on Recent Advances on Science and Engineering, Dubai, United Arab Emirates, 4–5 October 2023.

Abstract: Metal oxide semiconductor-based photocatalysis and advanced oxidation processes (AOPs) are effective in treating various recalcitrant pollutants such as organic dyes present in industrial wastewater streams. AOPs rely on the highly reactive hydroxyl radicals ($OH^{\bullet}$) that facilitate the non-selective destruction of most organic pollutants. Here, we present the novel synthesis of mesoporous $FeTiO_3$ catalyst via a simple, hard template-free, aqueous-solution-based hydrothermal synthesis method. The surfactant, tetradecyltrimethylammonium bromide (TTAB), was used as the structure-directing agent, the removal of which led to the formation of the mesoporous structure. The catalyst was characterized by thermo-gravimetric analysis (TGA), Fourier transform infrared spectroscopy (FTIR), Branauer–Emette–Teller analysis (BET), X-ray diffraction (XRD), and scanning electron microscope (SEM) techniques. The obtained catalyst has been studied for its photocatalytic application in the presence of H_2O_2 towards the degradation of organic dyes as representative pollutants, namely, rhodamine B (RhB) and methylene blue (MB) under direct solar light irradiation. The various characterizations confirm the formation of mesoporous $FeTiO_3$ with a pore size of ≈7.5 nm and a specific surface area of 65 ± 5 m^2/g. The influence of H_2O_2 oxidant on the removal of the said dyes has also been studied at various concentrations in the presence of the synthesized catalyst to determine the optimum dosage of H_2O_2. The catalyst was efficient in the complete synergistic adsorption-led photo-Fenton-like removal of MB in just 30 min of irradiation time, while the 96% RhB was degraded in 240 min. Moreover, this catalyst has also shown potential for fluoride adsorption that reaches up to more than 50% in 90 min.

Keywords: photocatalysis; mesoporous; wastewater treatment; fluoride adsorption

check for updates

Citation: Gupta, N.; Sarkar, A.; Pradhan, B.; Biswas, S.K. Hydrothermal Synthesis of Mesoporous $FeTiO_3$ for Photo-Fenton Degradation of Organic Pollutants and Fluoride Adsorption. *Eng. Proc.* **2023**, *59*, 134. https://doi.org/10.3390/engproc2023059134

Academic Editors: Nithesh Naik, Rajiv Selvam, Pavan Hiremath, Suhas Kowshik CS and Ritesh Ramakrishna Bhat

Published: 30 December 2023

Copyright: © 2023 by the authors. Licensee MDPI, Basel, Switzerland. This article is an open access article distributed under the terms and conditions of the Creative Commons Attribution (CC BY) license (https://creativecommons.org/licenses/by/4.0/).

1. Introduction

AOPs, like photocatalysis, photo-Fenton, and Fenton reactions, have emerged as highly effective methods for pollutant remediation due to their ability to generate potent radical species like $OH^{\bullet}$ radicals. Among these processes, photo-Fenton degradation involves the interaction of Fe^{3+}/Fe^{2+} ions with H_2O_2 to produce highly oxidizing $OH^{\bullet}$ radicals. In this context, Fe-containing heterogeneous photocatalysts are preferable for several reasons. Firstly, unlike homogeneous photo-Fenton processes, they avoid the problem of generating iron sludge [1]. Secondly, the bandgap excitation of the Fe-containing photocatalyst enhances the cycling between Fe^{3+}/Fe^{2+} centers, accelerating the generation of $OH^{\bullet}$ radicals [2].

$FeTiO_3$ or ilmenite is a suitable candidate for exploring such possibilities as it is a photoactive material having an energy band gap of ≈2.5–2.9 eV, capable of harnessing visible or solar light [3]. Ilmenite is abundantly available in the Earth's crust, which makes

it a potential catalyst for large-scale application in the degradation of industrial pollutants. Photocatalytic applications of $FeTiO_3$ have been explored before [3–5], but the problem of fast charge recombination impedes the required photocatalytic performance [6]. Moreover, previous studies on the photo-Fenton-like activity of ilmenite conducted at acidic pH resulted in the leaching of the Fe from $FeTiO_3$/ilmenite [6,7].

Here, we present a novel approach to synthesizing mesoporous $FeTiO_3$ using a simple aqueous solution-based method, which incorporates a soft templating technique, that has not been reported in the literature and showcases its excellent performance as a photo-Fenton catalyst for dye removal. Additionally, the porous nature of the synthesized material presents a valuable prospect for addressing fluoride contamination in drinking water. Given that fluoride levels exceeding 1.5 mg/L in drinking water are deemed unsafe for consumption [8], fluoride concentrations above the recommended limit can lead to serious health issues, such as fluorosis, making the development of efficient fluoride removal materials of significant importance [9].

2. Materials and Methods

Ferric nitrate nonahydrate ($Fe(NO_3)_3 \cdot 9H_2O$), TTAB, tartaric acid ($C_4H_6O_6$), potassium fluoride (KF), ammonium hydroxide (NH_4OH), and MB were purchased from Thomas Baker, Mumbai, India and titanium dioxide (TiO_2), hydrofluoric acid (HF), and RhB were purchased from Merck, Mumbai, India. All the reagents were used without any prior purification.

The material was characterized using the following characterization techniques:

Characterization of surface area and pore size were performed on Autosorb-iQ (Quantochrome, Boynton Beach, FL, USA) using BET and BJH (Barret–Joyner–Halend) methods, respectively. Thermal analysis was performed by TGA using the Perkin-Elmer Simultaneous Thermal Analyzer, (PerkinElmer, Inc., Waltham, MA, USA) at 5 °C/min heating rate. The FTIR spectra were recorded on the Shimadzu IRAffinity-1S FTIR Spectrophotometer (Shimadzu Corporation, Kyoto, Japan). XRD was performed using the X'Pert-pro diffractometer (PANalytical, Almelo, Netherlands). The microstructure analysis was carried out using JEOL-JSM6500 SEM (Jeol, Tokyo, Japan). The degradation of the dyes was monitored with the Shimadzu UV-1900i (Shimadzu Corporation, Kyoto, Japan) spectrophotometer. A MEX-TECH LX 1010B digital LUX meter (Mumbai, India) was used to measure the intensity of light irradiation. The measurement of fluoride concentration was conducted using the Hanna iris visible spectrophotometer HI801-02, (Hanna Instruments Inc., Woonsocket, RI, USA) with fluoride LR (0.00 to 2.00) mg/L as the standard.

Initially, the metal precursor solutions were prepared. The preparation of titanium tartrate precursor solution is mentioned elsewhere [10]. Then, 0.5 mmol $Fe(NO_3)_3 \cdot 9H_2O$ was dissolved in 5 ml of distilled water. A total of 0.15 mmol TTAB was dissolved in 9 mL of water. The above solutions were mixed to form a homogeneous mixture. The required amount of titanium tartrate solution (0.089 M) was concentrated at 25 mL and added to the mixture of $Fe(NO_3)_3 \cdot 9H_2O$ and TTAB. After that, the mixture was poured into an aqueous ammonia solution, and pH 9 was maintained. The solution mixture was stirred further on a magnetic stirrer for 7 h and heated for 1 h on a hot plate at 60 °C. The obtained mixture was poured into a Teflon-lined stain steel autoclave and kept for 12 h at 130 °C inside a hot air oven. The autoclave was naturally cooled, and the obtained product was evaporated in a hot water bath at 80 °C. The obtained powder was ground in a motor pestle and further calcined at 500 °C for 5 h in a muffle furnace.

The photocatalytic performance was measured under direct sunlight irradiation. A total of 50 mL of the dye solutions (RhB, MB), 1×10^{-5} M, was taken in a borosilicate beaker of 250 mL volume. A total of 50 mg of catalyst was added to the dye solution and kept in the dark under constant stirring for 1 h on a magnetic stirrer to establish the adsorption-desorption equilibrium. To find the percentage of degradation, 3.5 mL aliquots were taken from the solution every hour. For photo-Fenton experiments, the required amount of H_2O_2 was added to the solution containing dye and the catalyst prior to irradiation.

For fluoride ion adsorption, a standard fluoride solution (2 mg/L) was prepared in distilled water. The fluoride adsorption test was performed with an adsorbent dose of 0.07 g/100 mL, varying the adsorption time from 15 to 90 min. A certain amount of sample was taken out at the indicated time intervals and centrifuged to remove the adsorbent. In a cuvette, 2 mL of fluoride low-range reagent (H193729-0) was added, and using a plastic pipette, the cuvette was filled to the 10 mL mark with the extracted samples. The solution was mixed thoroughly and then placed into the instrument. The concentration of fluoride ions was measured using the Hanna Iris visible spectrophotometer with an accuracy of ± 0.03 mg/L $\pm$ 3% of the reading at room temperature.

The following formula was used to determine the percentage removal of dyes and fluoride:

$$\% \text{ Removal} = [C_0 - C/C_0] \times 100 \quad (1)$$

The Langmuir–Hinshelwood (L-H) model (Equation (2)) described the kinetics of RhB and MB degradation (Equation (2)).

$$\ln(C_0/C) = kt \quad (2)$$

where C_0 and C are the initial and final concentrations of dyes, respectively; t represents the reaction time expressed in min; and k denotes the pseudo-first-order rate constant for the degradation reaction. The pseudo-first-order rate constant (k) was determined from the slope of ln (C_0/C) versus t.

3. Results and Discussion

3.1. Characterization of $FeTiO_3$ Photocatalyst

In the synthesis of the $FeTiO_3$, TTAB surfactant was used as a soft template to create the mesoporous structure. In synthesis involving soft templates, the organic surfactants are initially arranged to form self-assemblies. After the addition of the inorganic phase (i.e., the metal precursors), the organic surfactant and the inorganic phase form an organic–inorganic structure such that the inorganic precursors cover the surfactant self-assemblies that remain embedded inside the inorganic phase [11]. On removal of these surfactant self-assemblies via thermal decomposition, voids are created in the place of the surfactant assemblies generating the desired pores [12].

Figure 1a shows the TGA plot of the as-synthesized sample. There was an initial weight loss of ≈14% up to 200 °C. This weight loss was related to the removal of adsorbed water. Upon further heating, a substantial reduction in weight, approximately 78%, was observed between 200 °C and 450 °C. This weight loss was primarily due to the thermal-decomposition-driven elimination of the organic reagents and surfactants employed in the synthesis process. No substantial weight loss was observed beyond 450 °C. This confirmed the complete removal of all the organic matter from the sample at temperatures beyond 450 °C and the formation of the pure compound. Thus, the samples were calcined at 500 °C and 600 °C to study their catalytic activities. The outcomes derived from the TGA analysis were further reestablished by the FTIR spectra of samples subjected to calcination at varying temperatures, as illustrated in Figure 1b. In the figure, spectrum a represents the FTIR spectra of pure TTAB surfactant. The as-synthesized sample (spectrum B) contains the FTIR peaks related to the symmetric and asymmetric stretching of alkyl C-H bonds of TTAB at 2850 cm^{-1} and 2920 cm^{-1} respectively, which confirms the presence of TTAB in the as-synthesized material [13]. On heating the sample at 200 °C (spectrum C), the peaks between 2700 cm^{-1} and 3500 cm^{-1} disappeared, indicating the removal of adsorbed water, as reflected in the TGA plot. The FTIR spectra of samples heated successively at 400 °C and 500 °C (spectrums D and E) reflect the complete removal of the surfactant or any organic remnants as all FTIR peaks observed for TTAB disappeared. The observed peaks in curves D and E positioned at 517 cm^{-1} and 430 cm^{-1} corresponded to Fe-O and Ti-O, respectively [14]. This indicates the presence of Fe-O and Ti-O bonds in the catalyst.

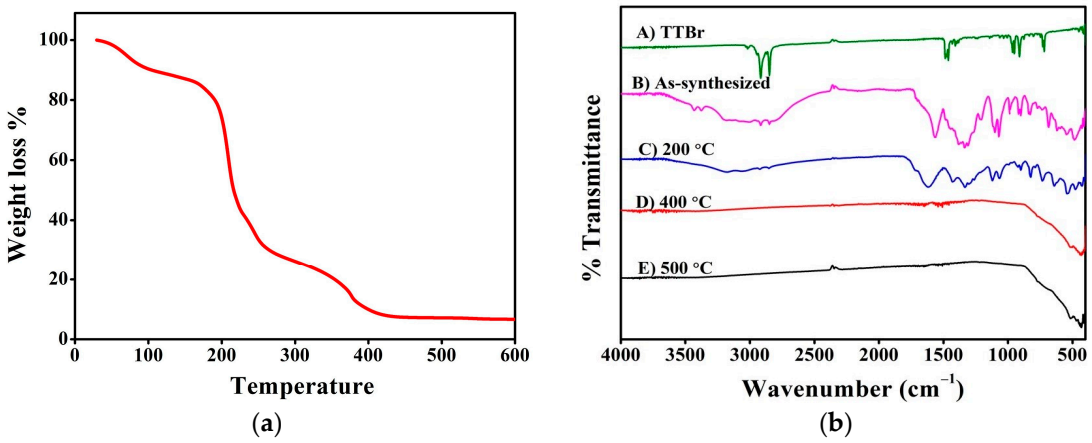


Figure 1. (**a**) TGA plot of as-synthesized $FeTiO_3$. (**b**) Comparison of FTIR spectra of $FeTiO_3$ calcined at various temperatures and TTAB surfactant.

The powder XRD measurement was used to verify the crystalline phase and structure of the synthesized $FeTiO_3$ catalyst. Figure 2a shows the XRD patterns of $FeTiO_3$ calcined at 500 °C and 600 °C. In both the samples heated at two different temperatures, sharp diffraction peaks indicate the crystalline nature of the prepared material. The major XRD diffraction peaks at 2θ values 24.4°, 33.3°, 35.8°, 41.1°, 49.8°, 54.4°, 57.1°, 62.8°, and 64.2° can be indexed to (012), (104), (110), (113), (024), (116), (018), (124), and (300) lattice planes, respectively (JCPDS card no. 75-1207) [3]. The observed diffraction peaks confirmed the presence of the hexagonal phase of $FeTiO_3$. N_2 adsorption–desorption experiments were performed using the multipoint BET model. The results in Figure 2b show a characteristic curve indicative of a mesoporous material. The surface area calculated was found to be 65 ± 5 m^2/g. Further, the inset in Figure 2b shows the pore size distribution of the mesoporous catalyst. The average pore size determined by the BJH model was found to be ≈7.5 nm.

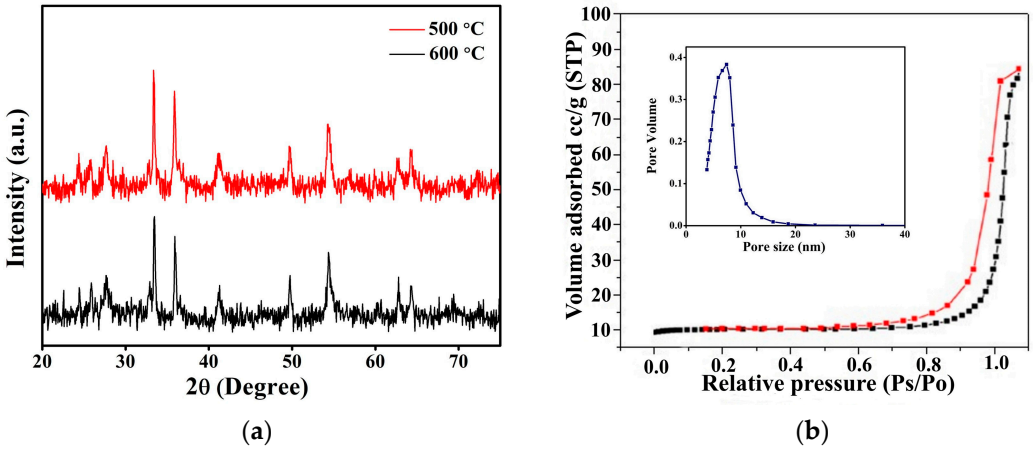


Figure 2. (**a**) XRD patterns of $FeTiO_3$ calcined at different temperatures. (**b**) N_2 adsorption–desorption isotherm of $FeTiO_3$ calcined at 500 °C.

SEM analysis was employed for the morphological characterization of $FeTiO_3$. Figure 3 shows the SEM micrographs of the samples calcined at 500 °C. It can be observed that the catalyst was made of agglomerated particles of irregular morphology. The particle size ranged from sub-microns to several micrometers. At higher magnification, it was seen that the surface of the $FeTiO_3$ catalyst contained pores of different sizes.

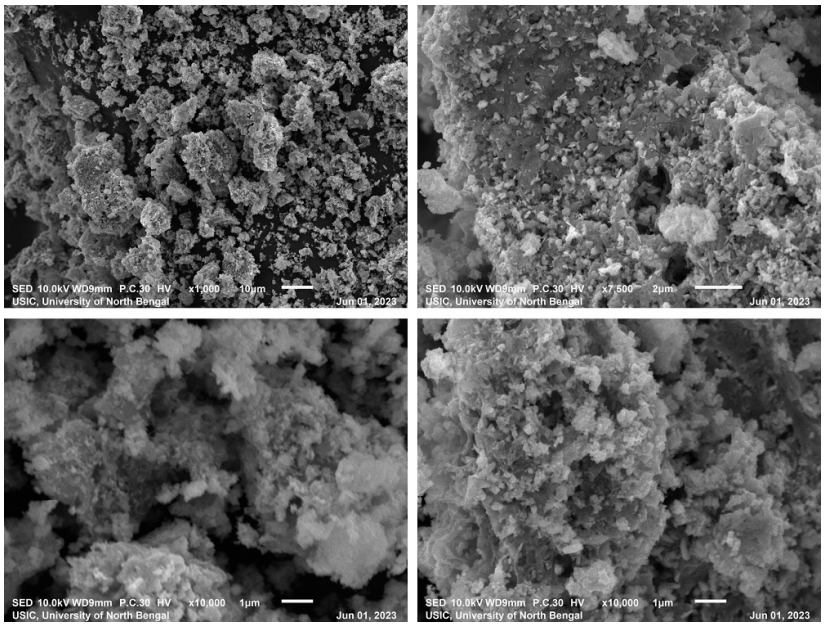


Figure 3. SEM images of $FeTiO_3$ composites calcined at 500 °C.

3.2. Catalytic Activity of $FeTiO_3$

Initially, the catalytic performance of samples calcined at 500 °C and 600 °C was compared to determine the effect of calcination temperature on their catalytic performance. In this study, the degradation of RhB dye, employed as a representative pollutant model, was investigated using $FeTiO_3$ under the influence of both H_2O_2 and solar light irradiation. Figure 4a shows the temporal changes in the characteristic peak of RhB at 554 nm recorded for 3 h of reaction time. The catalyst calcined at 500 °C showed slightly higher degradation of RhB (≈90%) at 3 h compared to that calcined at 600 °C (≈88%). It is already known that catalysis is a surface phenomenon. So, the more exposed surface-active sites, the more efficient the reaction will be. However, it has been observed that as the calcination temperature increases, the degree of aggregation also increases [15]. This would result in the agglomeration of smaller particles into larger particles, which explains the reduction in catalytic activity of the $FeTiO_3$ catalyst on increasing the calcination temperature. Therefore, in the present study, all the catalytic tests were carried out using $FeTiO_3$ calcined at 500 °C. H_2O_2 was utilized here as an oxidant to produce OH• radicals that are capable of degrading most organic compounds, owing to their high oxidation potential [16]. Thus, several concentrations of 15 mM, 25 mM, 35 mM, and 45 mM of H_2O_2 were utilized in the degradation of RhB dye in the presence of $FeTiO_3$ and solar irradiation to establish the optimal dosage of H_2O_2 required for the degradation. According to Figure 4b, when the concentration of H_2O_2 changed from 15 to 35 mM, the degradation efficiency also increased, going from 68% to 96% in the course of the 4 h reaction period. Because the amount of H_2O_2 used determines the concentration of OH• radicals generated in the reaction medium, it follows that as H_2O_2 concentration rises, more OH• radicals are generated, which increases degradation efficiency. Increasing the concentration from 35 mM to 45 mM caused a decrease in the degradation to 90%. The reason for such observation is the self-scavenging of the OH• radicals by the excess OH• radicals [17]. Thus, 35 mM H_2O_2 was determined as the optimal concentration.

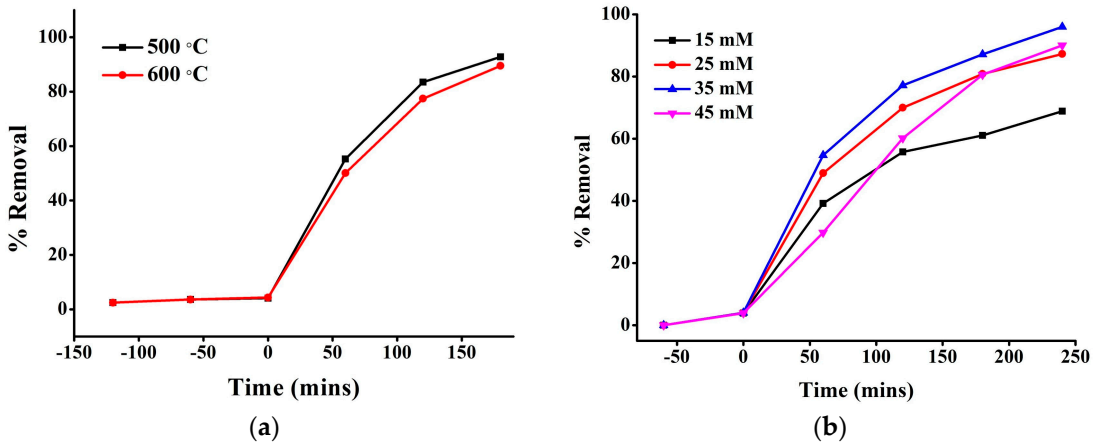


Figure 4. Effect of (**a**) calcination temperature and (**b**) different H_2O_2 concentrations on the degradation of RhB dye.

Figure 5a represents the time-dependent degradation of RhB using 35 mM H_2O_2, and 50 mg of $FeTiO_3$ catalyst, under natural sunlight. The absorbance maxima of RhB at 554 nm steadily decreased with the increasing reaction time and almost disappeared after 4 h of irradiation, and no shift in this peak was observed, indicating that no side products or intermediates were formed during the degradation. Thus, it was concluded that the degradation of RhB led to the complete breakdown of the conjugated molecule of RhB, leading to its mineralization. The degradation of another organic pollutant dye, MB, was also carried out in the same catalytic condition as mentioned above. Figure 5b depicts the time-dependent degradation of MB in the presence of $FeTiO_3$, H_2O_2, and light. In comparison to RhB, it was found that a higher percentage of MB, about 50%, was absorbed on the catalyst, while such adsorption was not obtained in the case of RhB. Considering the molecular structure of MB and RhB, MB is a planar molecule and smaller in size compared to RhB [18]. Thus, it makes it easier for MB to diffuse into the pores of the catalyst, leading to a higher degree of adsorption. Again, as a greater number of MB molecules are adsorbed on the surface of the catalyst, its degradation progresses more swiftly because of better charge transfer, leading to its complete removal in just 30 min of reaction time. The plot of ln (C_0/C) vs. t shows a good fit with $R^2 > 0.95$, indicating that the degradation follows the pseudo-first-order kinetic, and the rate constants were found to be 0.013 min^{-1} and 0.12176 min^{-1} for the degradation of RhB and MB dyes, respectively.

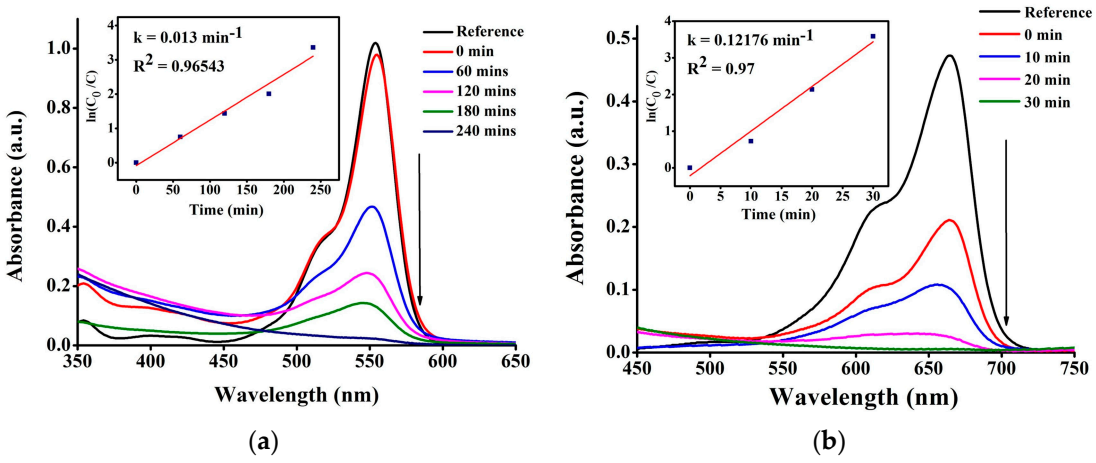


Figure 5. Degradation of (**a**) RhB and (**b**) MB in the presence of H_2O_2, $FeTiO_3$, and direct solar irradiation.

Further, the photocatalytic, Fenton, and H_2O_2-led degradation of RhB was performed to compare and determine the role of the combined catalytic components, i.e., catalyst and

light, catalyst and H_2O_2, and only H_2O_2, respectively, with the photo-Fenton removal of RhB dye shown in Figure 6a. Maximum degradation close to 100% was attained during the photo-Fenton process, i.e., in the presence of $FeTiO_3$ and H_2O_2 under solar light irradiation. As evident from the observations, the least degradation of about 6% was induced by H_2O_2. This can be explained by the fact that H_2O_2 does not generate any OH• radicals on its own [19]. It can be decomposed to OH• radical by the action of light, preferably in the UV range (Equation (5)), or it can be activated by Fe^{2+}/Fe^{3+} ions present on the surface of the catalyst (represented as $\equiv Fe^{3+}/\equiv Fe^{2+}$) to generate OH• radicals (Equations (2)–(4)) [16]. This indicates that only H_2O_2 alone is not sufficient to drive the degradation process. Next, during the photocatalytic degradation experiment, a small amount of degradation (16%) was observed. The photocatalysts, on light irradiation, generated active species like electrons and holes on bandgap excitation (Equation (6)) that further produced reactive radicals to degrade organic pollutants (Equations (7) and (8)) [6]. The observed degradation was a result of such band gap excitation. On the other hand, the low efficiency of degradation could be explained by the fast recombination of electron-hole pairs. The contribution of the Fenton process in the absence of any light by the action of the catalyst and H_2O_2 was also investigated to determine the role of light irradiation on dye removal. The Fenton process also brought about 15% degradation of RhB after 4 h. It can be concluded that light is an important catalytic component in the observed degradation of RhB. These results indicate that the $FeTiO_3$ catalyst, H_2O_2, and light synergistically enhance the dye degradation process and are required for the removal of the said dye. Moreover, the catalyst showed up to 95% degradation after three catalytic cycles for the degradation of RhB, as observed in Figure 6b, indicating the stability of the synthesized catalyst for repeated use.

$$\equiv Fe^{3+} + H_2O_2 \rightarrow \equiv Fe^{3+} + HO_2^{\bullet} + H^+ \quad (3)$$

$$\equiv Fe^{2+} + H_2O_2 \rightarrow \equiv Fe^{3+} + OH^{\bullet} + OH^- \quad (4)$$

$$H_2O_2 + \text{light} \rightarrow OH^{\bullet} + OH^- \quad (5)$$

$$FeTiO_3 + \text{light} \rightarrow e^-{}_{cb} + h^+{}_{vb} \quad (6)$$

$$e^-{}_{cb} + O_2 \rightarrow O_2{}^{-\bullet} \quad (7)$$

$$h^+{}_{vb} + H_2O \rightarrow OH^{\bullet} + H^+ \quad (8)$$

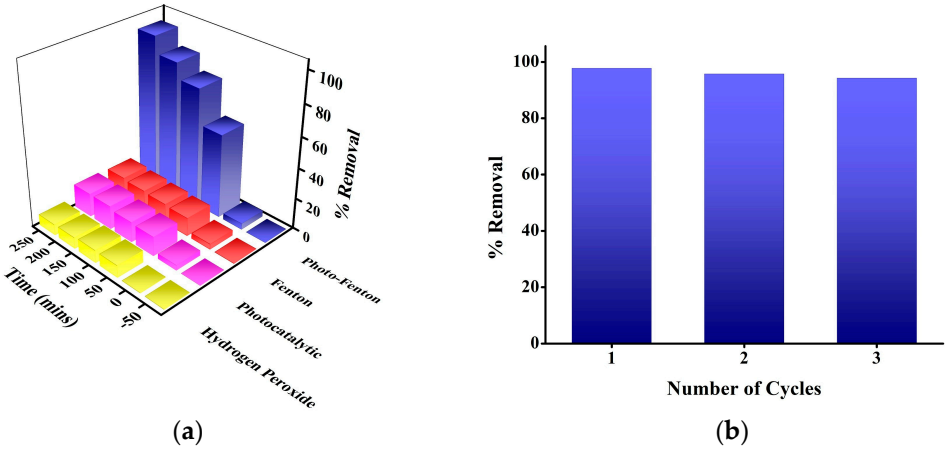


Figure 6. (**a**) Comparison of RhB degradation by different catalytic setups. (**b**) Recyclability test of $FeTiO_3$ during the degradation of RhB dye.

Additionally, the synthesized mesoporous $FeTiO_3$ was used for the removal of fluoride ions from water at neutral pH as an adsorbent. Figure 7 shows the changes in the fluoride concentration during 90 min of adsorption. There was a maximum fluoride removal of >40% in the initial 15 min of adsorption. After 30 min, the fluoride removal % slowed

down, and at 60 min of adsorption, saturation was attained following the establishment of the adsorption–desorption equilibrium. At an initial fluoride concentration of 2 mg/L and neutral pH, the $FeTiO_3$ adsorbent achieved a maximum fluoride adsorption percentage of 55% and an adsorption capacity of 1.5 mg/g. According to WHO recommendations, fluoride concentration >1.5 mg/L is unfit for consumption. However, the research on fluoride adsorption is generally conducted at higher concentrations ranging from 5 mg/L and above, and it has been found that the adsorbent's ability to adsorb fluoride decreases at low concentrations [20]. Our adsorbent demonstrated significant fluoride adsorption ability even at low fluoride concentrations of 2 mg/L and without pH adjustment, which indicates the potential applicability of $FeTiO_3$ in fluoride adsorption.

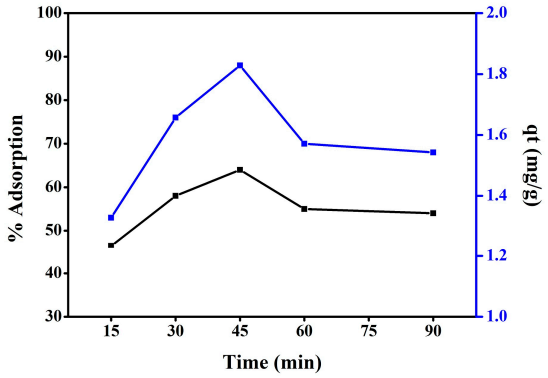


Figure 7. Fluoride adsorption using $FeTiO_3$ as adsorbent.

4. Conclusions

In the present study, TTAB served as the structure-directing agent or the template. On thermal treatment at temperatures >200 °C as observed from the TGA and FTIR studies, the template, namely, TTAB, was decomposed, creating the mesoporous structure, without the need for any hard templates. The synthesized mesoporous $FeTiO_3$ was found to be an effective catalyst in the photo-Fenton degradation of organic dyes such as RhB and MB. The mesoporous nature of the prepared material also makes it a suitable adsorbent for fluoride adsorption as found in this study. However, various factors influence the extent of adsorption such as the solution pH, adsorbent dosages, interfering ions, etc. These can be explored in the future.

Author Contributions: Conceptualization, S.K.B. and A.S.; methodology, N.G. and B.P.; software, N.G.; validation, S.K.B. and A.S.; formal analysis, S.K.B. and N.G.; investigation, N.G. and B.P.; resources, S.K.B.; data curation, N.G. and B.P.; writing—N.G. and S.K.B.; writing—review and editing, S.K.B. and A.S.; visualization N.G.; supervision, S.K.B. and A.S.; project administration, S.K.B.; funding acquisition, S.K.B. and N.G. All authors have read and agreed to the published version of the manuscript.

Funding: S.K.B. would like to acknowledge the TMA Pai research grant of Sikkim Manipal University for financial support to this research project work.

Institutional Review Board Statement: Not applicable.

Informed Consent Statement: Not applicable.

Data Availability Statement: The data generated in this study are presented in the article.

Acknowledgments: N.G. would like to acknowledge the TMA Pai research fellowship of Sikkim Manipal University for providing financial assistance to the scholar.

Conflicts of Interest: The authors declare no conflicts of interest.

References

1. Hamd, W.S.; Dutta, J. Heterogeneous photo-Fenton reaction and its enhancement upon addition of chelating agents. In *Micro and Nano Technologies, Nanomaterials for the Detection and Removal of Wastewater Pollutants*; Bonelli, B., Freyria, F.S., Rossetti, I., Sethi, R., Eds.; Elsevier: Amsterdam, The Netherlands, 2020; pp. 303–330. [CrossRef]
2. Chen, S.; Wu, Y.; Li, G.; Wu, J.; Meng, G.; Guo, X.; Liu, Z. A novel strategy for preparation of an effective and stable heterogeneous photo-Fenton catalyst for the degradation of dye. *Appl. Clay Sci.* **2017**, *136*, 103–111. [CrossRef]
3. Moradi, M.; Vasseghian, Y.; Khataee, A.; Harati, M.; Arfaeinia, H. Ultrasound-assisted synthesis of $FeTiO_3$/GO nanocomposite for photocatalytic degradation of phenol under visible light irradiation. *Sep. Purif. Technol.* **2021**, *261*, 118274. [CrossRef]
4. Zhang, S.T.; Ruan, Y.R.; Liu, C.; Wang, P.; Ma, Y.Q. The evolution of structure, chemical state and photocatalytic performance of α-Fe/$FeTiO_3$/TiO_2 with the nitridation at different temperatures. *Mater. Res. Bull.* **2017**, *95*, 503–508. [CrossRef]
5. Truong, Q.D.; Liu, J.Y.; Chung, C.C.; Ling, Y.C. Photocatalytic reduction of CO_2 on $FeTiO_3$/TiO_2 photocatalyst. *Catal. Commun.* **2012**, *19*, 85–89. [CrossRef]
6. García-Muñoz, P.; Pliego, G.; Zazo, J.A.; Bahamonde, A.; Casas, J.A. Ilmenite ($FeTiO_3$) as low cost catalyst for advanced oxidation processes. *J. Environ. Chem. Eng.* **2016**, *4*, 542–548. [CrossRef]
7. Pataquiva-Mateus, A.Y.; Zea, H.R.; Ramirez, J.H. Degradation of orange II by Fenton reaction using ilmenite as catalyst. *Environ. Sci. Pollut. Res.* **2017**, *24*, 6187–6194. [CrossRef] [PubMed]
8. Mukherjee, A.; Adak, M.K.; Upadhyay, S.; Khatun, J.; Dhak, P.; Khawas, S.; Ghorai, U.K.; Dhak, D. Efficient fluoride removal and dye degradation of contaminated water using Fe/Al/Ti oxide nanocomposite. *ACS Omega* **2019**, *4*, 9686–9696. [CrossRef] [PubMed]
9. Kabir, H.; Gupta, A.K.; Tripathy, S. Fluoride and Human Health: Systematic appraisal of sources, exposures, metabolism, and toxicity. *Crit. Rev. Environ. Sci. Technol.* **2020**, *5*, 1116–1193. [CrossRef]
10. Sen, S.; Choudhary, R.N.P.; Tarafdar, A.; Pramanik, P. Novel technique for synthesis and characterization of nanosized $Ba_{1-X}Sr_xSn_{0.15}Ti_{0.85}O_3$ ceramics. *Phys. Status Solidi (a)* **2004**, *201*, 937–943. [CrossRef]
11. Poolakkandy, R.R.; Menamparambath, M.M. Soft-Template-Assisted Synthesis: A promising approach for the fabrication of transition metal oxides. *Nanoscale Adv.* **2020**, *2*, 5015–5045. [CrossRef] [PubMed]
12. Li, C.; Yang, W.; He, W.; Zhang, X.; Zhu, J. Multifunctional surfactants for synthesizing high-performance energy storage materials. *Energy Storage Mater.* **2021**, *43*, 1–19. [CrossRef]
13. Dubey, N.; Arora, S. Surfactant assisted synthesis of pH responsive polyaniline-cellulose biocomposite for sensor applications. *Polym. Plast. Technol. Mater.* **2021**, *60*, 1135–1147. [CrossRef]
14. Kumar, M.R.A.; Abebe, B.; Nagaswarupa, H.P.; Murthy, H.C.A.; Ravikumar, C.R.; Sabir, F.K. Enhanced photocatalytic and electrochemical performance of TiO_2-Fe_2O_3 nanocomposite: Its applications in dye decolorization and as supercapacitors. *Sci. Rep.* **2020**, *10*, 1249. [CrossRef] [PubMed]
15. Phromma, S.; Wutikhun, T.; Kasamechonchung, P.; Eksangsri, T.; Sapcharoenkun, C. Effect of calcination temperature on photocatalytic activity of synthesized TiO_2 nanoparticles via wet ball milling sol-gel method. *Appl. Sci.* **2020**, *10*, 993. [CrossRef]
16. Sarkar, A.; Gupta, N.; Biswas, S.K. Bimodal mesoporous α-Fe_2O_3/SiO_2 composite: A highly efficient heterogeneous solar-driven photo-Fenton catalyst. *J. Mol. Struct.* **2023**, *1284*, 135373. [CrossRef]
17. Zhou, L.; Lei, J.; Wang, L.; Liu, Y.; Zhang, J. Highly efficient photo-Fenton degradation of methyl orange facilitated by slow light effect and hierarchical porous structure of Fe_2O_3-SiO_2 photonic crystals. *Appl. Catal. B* **2018**, *237*, 1160–1167. [CrossRef]
18. Taher, T.; Yoshida, A.; Lesbani, A.; Kurnia, I.; Guan, G.; Abudula, A.; Ueda, W. Adsorptive removal and photocatalytic decomposition of cationic dyes on niobium oxide with deformed orthorhombic structure. *J. Hazard. Mater.* **2021**, *41*, 125635. [CrossRef] [PubMed]
19. Boczkaj, G.; Fernandes, A. Wastewater treatment by means of advanced oxidation processes at basic pH conditions: A review. *Chem. Eng. J.* **2017**, *320*, 608–633. [CrossRef]
20. Habuda-Stanić, M.; Ravančić, M.; Flanagan, A. A review on adsorption of fluoride from aqueous solution. *Materials* **2014**, *7*, 6317–6366. [CrossRef] [PubMed]

Disclaimer/Publisher's Note: The statements, opinions and data contained in all publications are solely those of the individual author(s) and contributor(s) and not of MDPI and/or the editor(s). MDPI and/or the editor(s) disclaim responsibility for any injury to people or property resulting from any ideas, methods, instructions or products referred to in the content.